

**Negligible oxygen vacancies, low critical current density, electric-field modulation, in-plane anisotropic and high-field transport of a superconducting Nd<sub>0.8</sub>Sr<sub>0.2</sub>NiO<sub>2</sub>/SrTiO<sub>3</sub> heterostructure**

Xiaorong Zhou<sup>1,#</sup>, Zexin Feng<sup>1,#</sup>, Peixin Qin<sup>1</sup>, Han Yan<sup>1</sup>, Xiaoning Wang<sup>1</sup>, Pan Nie<sup>2</sup>, Haojiang Wu<sup>1</sup>, Xin Zhang<sup>1</sup>, Hongyu Chen<sup>1</sup>, Ziang Meng<sup>1</sup>, Zengwei Zhu<sup>2,3</sup>, Zhiqi Liu\*

1. *School of Materials Science and Engineering, Beihang University, Beijing 100191, China*

2. *Wuhan National High Magnetic Field Center, Huazhong University of Science and Technology, Wuhan 430074, China*

3. *School of Physics, Huazhong University of Science and Technology, Wuhan 430074, China*

<sup>#</sup>These authors contributed equally to this work.

Email: zhiqi@buaa.edu.cn

**The emerging Ni-based superconducting oxide thin films are rather intriguing to the entire condensed matter physics. Here we report some brief experimental results on transport measurements for a 14-nm-thick superconducting Nd<sub>0.8</sub>Sr<sub>0.2</sub>NiO<sub>2</sub>/SrTiO<sub>3</sub> thin-film heterostructure with an onset transition temperature of ~9.5 K. Photoluminescence measurements reveal that there is negligible oxygen vacancy creation in the SrTiO<sub>3</sub> substrate during thin-film deposition and post chemical reduction for the Nd<sub>0.8</sub>Sr<sub>0.2</sub>NiO<sub>2</sub>/SrTiO<sub>3</sub> heterostructure. It was found that the critical current density of the Nd<sub>0.8</sub>Sr<sub>0.2</sub>NiO<sub>2</sub>/SrTiO<sub>3</sub> thin-film heterostructure is relatively small, ~4×10<sup>3</sup> A/cm<sup>2</sup>. Although the surface steps of SrTiO<sub>3</sub> substrates lead to an anisotropy for in-plane resistivity, the superconducting transition temperatures are almost the same. The out-of-plane magnetotransport measurements yield an upper critical field of ~11.4 T and an estimated in-plane Ginzburg-Landau coherence length of ~5.4 nm. High-field magnetotransport measurements up to 50 T reveal anisotropic critical fields at 1.8 K for three different measurement geometries and a complicated Hall effect. An electric field applied via the SrTiO<sub>3</sub> substrate slightly varies the superconducting transition temperature. These experimental results could be useful for this rapidly developing field.**

The recent observation of superconductivity in  $\text{Nd}_{0.8}\text{Sr}_{0.2}\text{NiO}_2$  thin films has attracted explosive interests owing to the possible similarity of electronic structures between the nickelates and high- $T_c$  cuprate superconductors [1]. However, it is found that the parent compound  $\text{NdNiO}_2$  of the superconducting  $\text{Nd}_{0.8}\text{Sr}_{0.2}\text{NiO}_2$  lacks in any magnetic order down to 1.7 K [2], which is different from superconducting cuprates where the antiferromagnetic ordering of parent compounds is important to high temperature superconductivity [3]. Hence, the superconductivity in  $\text{Nd}_{0.8}\text{Sr}_{0.2}\text{NiO}_2$  thin films could be a new type of superconducting phenomenon that will help us understand the nature of the high-temperature superconductivity better.

Although there are various theoretical works on this new superconducting system [4-28], only a few experimental results were reported. As far as we have noticed, there are only four groups claiming successful synthesis of nanoscale superconducting  $\text{Nd}_{0.8}\text{Sr}_{0.2}\text{NiO}_2$  thin films. Specifically, most of the experimental work [1, 29-32] in this area came from the same Stanford group who first realized this phenomenon. Additionally, Gu *et al.* [33] and Xiang *et al.* [34] from Nanjing University studied the superconducting gaps via scanning tunneling microscopy spectroscopy and physical properties by transport measurements. Moreover, Gao *et al.* [35] from Institute of Physics, Chinese Academy of Sciences reported the successful growth of superconducting infinite-layer  $\text{Nd}_{0.8}\text{Sr}_{0.2}\text{NiO}_2$  thin films by chemical reduction in a quartz tube and Zeng *et al.* [36] from National University of Singapore achieved the superconductivity in  $\text{Nd}_{0.8}\text{Sr}_{0.2}\text{NiO}_2$  thin films by reducing  $\text{Nd}_{0.8}\text{Sr}_{0.2}\text{NiO}_3$  thin films with  $\text{CaH}_2$  powder in a vacuum chamber at 340-360 °C for 80-120 mins. Especially, the chemical reduction carried out in a pulse laser deposition vacuum chamber by Zeng *et al.* could be much more feasible as most oxide electronics groups lack in experimental experience in dealing with chemical duction in Pyrex glass or quartz tube.

Based on the chemical reduction process reported by Zeng *et al.* [36] and our previous experimental results [37], we have successfully fabricated superconducting  $\text{Nd}_{0.8}\text{Sr}_{0.2}\text{NiO}_2$  films. Specifically, epitaxial 113-phase perovskite  $\text{Nd}_{0.8}\text{Sr}_{0.2}\text{NiO}_3$  thin films were grown on (001)-oriented  $\text{TiO}_2$ -terminated  $\text{SrTiO}_3$  single-crystal substrates

by a pulsed laser deposition system at 700 °C and 20 Pa oxygen partial pressure. Subsequently,  $\text{Nd}_{0.8}\text{Sr}_{0.2}\text{NiO}_3$  samples were contained in Al foils with each piece mixed with 0.1 g  $\text{CaH}_2$  powder and then moved to the pulsed laser deposition vacuum chamber. The chemical reduction was performed at 350 °C for 2 h. During this chemical reduction, the vacuum chamber was sealed without connecting to the turbo pump. The ramping rate for heating and cooling was kept at 10 °C/min.

In this article, we report photoluminescence measurement results and the transport properties of a 14-nm-thick  $\text{Nd}_{0.8}\text{Sr}_{0.2}\text{NiO}_2/\text{SrTiO}_3$  heterostructure, which include critical current density, electric-field modulation, in-plane anisotropy and high-field magnetotransport properties of such a superconducting system. We noticed that all these aspects have not been reported in previous experimental studies [1,29-36].

Figure 1 shows the photoluminescence spectra of the  $\text{Nd}_{0.8}\text{Sr}_{0.2}\text{NiO}_2/\text{SrTiO}_3$  heterostructure and a bare  $\text{SrTiO}_3$  substrate that was purchased from Crystec and used to fabricate  $\text{Nd}_{0.8}\text{Sr}_{0.2}\text{NiO}_2/\text{SrTiO}_3$  heterostructures. Oxygen vacancies in  $\text{SrTiO}_3$  typically lead to multiple defect photoluminescence peaks at a wavelength range between 350 and 600 nm and the intensity of the peaks are very sensitive to the concentration of oxygen vacancies [38,39]. Accordingly, the photoluminescence spectra could be used to qualitatively examine the oxygen vacancy concentration on the surface region of a bulk  $\text{SrTiO}_3$  single crystal. Compared with the photoemission signal of the bare  $\text{SrTiO}_3$  substrate that is supposed to possess only a tiny amount of oxygen vacancies, the defect-related in-gap photoemission of the superconducting  $\text{Nd}_{0.8}\text{Sr}_{0.2}\text{NiO}_2/\text{SrTiO}_3$  heterostructure becomes even weaker. This indicates that oxygen vacancies in the superconducting  $\text{Nd}_{0.8}\text{Sr}_{0.2}\text{NiO}_2/\text{SrTiO}_3$  heterostructure are negligible.

As the 113-phase  $\text{Nd}_{0.8}\text{Sr}_{0.2}\text{NiO}_3/\text{SrTiO}_3$  heterostructure was fabricated at a high oxygen partial pressure of 150 mTorr at 700°C in our pulsed laser deposition system, the deposition process could act as oxygen annealing for the  $\text{SrTiO}_3$  substrate used for the  $\text{Nd}_{0.8}\text{Sr}_{0.2}\text{NiO}_3$  film fabrication, which can thus lower the photoluminescence peak. On the other hand, after chemical reduction, the conducting film capping could suppress

the photoluminescence emission as well due to the absorption of photons by free electrons. In addition, the weaker photoemission intensity of the superconducting  $\text{Nd}_{0.8}\text{Sr}_{0.2}\text{NiO}_2/\text{SrTiO}_3$  heterostructure relative to the bare  $\text{SrTiO}_3$  substrate suggests that the post chemical reduction process for achieving the 112-phase  $\text{Nd}_{0.8}\text{Sr}_{0.2}\text{NiO}_2/\text{SrTiO}_3$  heterostructure does not produce noticeable oxygen vacancies as well. This experimental aspect could be rather useful to theoretically model the superconducting  $\text{Nd}_{0.8}\text{Sr}_{0.2}\text{NiO}_2/\text{SrTiO}_3$  heterostructure.

The temperature-dependent resistivity of the  $\text{Nd}_{0.8}\text{Sr}_{0.2}\text{NiO}_2/\text{SrTiO}_3$  heterostructure measured by the linear four-probe geometry is plotted in Fig. 2a. It shows metallic behavior at high temperature with a room-temperature resistivity of  $\sim 1.8 \text{ m}\Omega\cdot\text{cm}$ , which is comparable with that reported in Ref. [1]. The superconducting phase transition occurs at an onset transition temperature of  $\sim 9.5 \text{ K}$  and a zero-resistance state arises at  $\sim 3.0 \text{ K}$ . Figure 2b plots current-density-dependent resistance measured at different temperatures. The critical current density of the superconducting  $\text{Nd}_{0.8}\text{Sr}_{0.2}\text{NiO}_2$  film is  $\sim 4 \times 10^3 \text{ A/cm}^2$ , which is much smaller than that of some typical superconductors such as Nb ( $\sim 10^6 \text{ A/cm}^2$ ) [40],  $\text{YBa}_2\text{Cu}_3\text{O}_{7-x}$  ( $\sim 8 \times 10^6 \text{ A/cm}^2$ ) [41],  $\text{MgB}_2$  ( $\sim 10^6 \text{ A/cm}^2$ ) [42] and Fe-based superconductors ( $\sim 2 \times 10^6 \text{ A/cm}^2$ ) [43]. The critical current density of a superconductor is typically associated with the magnetic flux pinning. The relatively small value of the critical current density, corresponding to a weak pinning capability, could be an intrinsic property of superconducting  $\text{Nd}_{0.8}\text{Sr}_{0.2}\text{NiO}_2$  thin films. Alternatively, it may be related to the small thickness of the sample as a result of interfacial/surface scattering.

Up to now, the emerging Ni-based oxide superconductivity has not been achieved in bulk nickelates [44-46] such as  $\text{Nd}_{0.8}\text{Sr}_{0.2}\text{NiO}_2$ , which suggests that the surface or interfacial effects between the films and substrates may play an important role in this new superconducting phenomenon. It is worth emphasizing that our thin films were fabricated on buffered HF-treated  $\text{SrTiO}_3$  substrates that exhibit single  $\text{TiO}_2$  terminations. Due to the steps on the surfaces of  $\text{TiO}_2$ -terminated  $\text{SrTiO}_3$  substrates as a result of a vicinal miscut angle, we specifically investigated the effect of surface steps

on the electrical transport properties of the  $\text{Nd}_{0.8}\text{Sr}_{0.2}\text{NiO}_2/\text{SrTiO}_3$  thin-film heterostructure.

Our atomic force microscopy measurements reveal that the surface steps of  $\text{TiO}_2$ -terminated  $\text{SrTiO}_3$  substrates are almost parallel to one in-plane edge of the (001) plane. Therefore, we made linear four-probe electrical contacts with an Al wire bonder along two orthorhombic in-plane edges. The measurement geometry is schematized in Fig. 3a. As shown in Fig. 3b, the temperature-dependent resistivity for different measurement geometries exhibit anisotropic behavior and the room-temperature resistivity for the current direction perpendicular to  $\text{SrTiO}_3$  surface steps is  $\sim 7.7\%$  higher than that for the current direction parallel to  $\text{SrTiO}_3$  surface steps. This suggests that the electron scattering at the surface steps can remarkably increase the resistivity. However, the onset transition temperature is  $\sim 9.5$  K and  $\sim 10.0$  K for the current perpendicular and parallel to the surface steps, respectively, which are almost the same. It implies that although the surface steps could yield an intrinsic anisotropy in electrical transport of the normal state, they have a negligible effect for the superconducting state of the  $\text{Nd}_{0.8}\text{Sr}_{0.2}\text{NiO}_2/\text{SrTiO}_3$  thin-film heterostructure.

Subsequently, we performed out-of-plane magnetotransport measurements with static magnetic fields up to 9 T for the  $\text{Nd}_{0.8}\text{Sr}_{0.2}\text{NiO}_2/\text{SrTiO}_3$  thin-film heterostructure. The measurement geometry is illustrated in Fig. 4a. As shown in Fig. 4b, the superconductivity is suppressed by the increasing magnetic field but not completely destroyed up to 9 T, which indicates that the out-of-plane upper critical field is larger than 9 T. Furthermore, the half normal-state resistivity value was utilized to estimate the upper critical field  $\mu_0 H_{c2}(0 \text{ K})$ . As illustrated in Fig. 4c, the upper critical field at 0 K can be estimated based on the Werthamer-Helfand-Hohenberg formula [47]  $\mu_0 H_{c2}(0 \text{ K}) = -0.7T_c \left( \frac{d\mu_0 H_{c2}}{dT} \right)_{T_c}$ . As a result, the zero-temperature upper critical field is obtained to be  $\sim 11.37$  T. According to the Ginzburg-Landau equation [48]  $\mu_0 H_{c2}(0 \text{ K}) = \frac{\Phi_0}{2\pi\xi_{GL}^2(0 \text{ K})}$ , where  $\Phi_0$  is magnetic flux quantum, we obtain an in-plane Ginzburg-Landau coherence length of  $\sim 5.4$  nm.

We notice that high-magnetic-field transport properties of superconducting  $\text{Nd}_{0.8}\text{Sr}_{0.2}\text{NiO}_2/\text{SrTiO}_3$  thin-film heterostructures have not been reported either due to the lack of superconducting samples or limited high-field experiment equipment. To fill this research gap, we collaborated with an experimental group at Wuhan National High Magnetic Field Center, Huazhong University of Science and Technology [49] and performed systematic pulsed high-field magnetotransport measurements up to 50 T for the  $\text{Nd}_{0.8}\text{Sr}_{0.2}\text{NiO}_2/\text{SrTiO}_3$  thin-film heterostructure.

As shown in Fig. 5a, with increasing the pulsed magnetic field, the resistivity of the superconducting state at 1.8 K increases from zero to a finite value. At  $\sim 11.5$  T, the normal-state resistivity is achieved and afterwards the resistivity trends to saturate. For the normal state at 20 K (Fig. 5b), a small negative magnetoresistance exists for low fields. However, the magnetoresistance trends to become positive for high-fields, likely due to the regular Lorentz-force-related orbital scattering. As the weak localization related negative magnetoresistance is typically observed in two-dimensional electron systems, the negative magnetoresistance could be possibly be related to magnetic spins in the normal state of the  $\text{Nd}_{0.8}\text{Sr}_{0.2}\text{NiO}_2/\text{SrTiO}_3$  thin-film heterostructure.

For a thin-film superconductor, it is always interesting to examine whether the critical magnetic field to break the superconducting state is isotropic for out-of-plane and in-plane magnetic fields. Regarding this issue, it seems that different groups have acquired slightly different results. For example, the experimental research performed by the Stanford group [32] suggested that the upper critical field is isotropic for out-of-plane and in-plane magnetic fields, while the study conducted by the Nanjing University group [34] implied that the upper critical field is larger when the magnetic field is applied out of plane.

To clarify this issue, we performed high-field magnetoresistance measurements for three different geometries at the zero-resistance state 1.8 K. As shown in Fig. 6, when the magnetic field is applied out of plane, the critical field for achieving the saturated normal-state resistivity is  $\sim 11.5$  T, while it is  $\sim 14.5$  T for the magnetic field applied in plane regardless of the in-plane angle between the magnetic field and the measuring

current. The ~26% difference in the critical fields reflects that the out-of-plane magnetic field is easier to fully break the superconducting state via the Lorentz-force-related orbital scattering. In contrast, when the magnetic field is applied in plane, the orbital scattering is largely suppressed for a nanoscale thin film sample, it can only break the Cooper pair via the Zeeman alignment of two opposite spins. Our experimental results agree well with what the Nanjing University group has concluded [34].

From the first report [1], the emerging Ni-based oxide superconductor exhibit multiple-band transport as its Fermi surface involves both electron and hole pockets. To check it out, we performed pulsed high-field Hall measurements up to 50 T as well. The specific electrical connections are illustrated in Fig. 7a. The collected Hall voltage signals versus the magnetic field are plotted in Fig. 7b for different temperatures for the normal state above 10 K. Above 20 K, the Hall effect pertains to the *n*-type electron transport considering our measurement geometry in Fig. 7a and gradually becomes nonlinear at fields higher than ~20 T. At 20 K, the Hall effect is complicated by multiple curvature changes. Below 20 K, the Hall effect below 15 T corresponds to the *p*-type hole transport, but it changes significantly at higher fields later. All these data depict that the Fermi surface of the Nd<sub>0.8</sub>Sr<sub>0.2</sub>NiO<sub>2</sub>/SrTiO<sub>3</sub> thin-film heterostructure containing different types of pockets evolves with temperature and magnetic field.

The ground states of strongly correlated oxides are closely related to the carrier density. Accordingly, we further explored how the superconducting transition could possibly evolve with a perpendicular gating electric field applied onto the SrTiO<sub>3</sub> substrate, which can inject electrons/holes into the conducting Nd<sub>0.8</sub>Sr<sub>0.2</sub>NiO<sub>2</sub> thin-film channel. As SrTiO<sub>3</sub> has a rather large dielectric constant at low temperatures [50], the electrostatic tuning could be most effective for low temperatures, which is different from the piezoelectric strain modulation operated from at room temperature [51-61]. As a result, we have examined the temperature-dependent resistivity below 12 K for different gating electric fields  $E_G$ . As shown in Fig. 8, a negative electric field of -4 kV/cm that injects holes into slightly increases the superconducting transition temperature, while a positive electric field of +3.6 kV/cm decreases the onset

superconducting temperature by  $\sim 0.5$  K. Such a modulation is quite similar to the electric-field effect in superconducting  $\text{YBa}_2\text{Cu}_3\text{O}_7$  films [62]. Therefore, it is feasible to tune the superconducting phase transition of the Ni-based oxide superconductivity by electrostatic modulation, which could be further enhanced via ionic liquid modulation.

Up to now, the superconductivity has not been realized in bulk infinite-layer nickelates. If later possibly achieved, the critical current densities of bulk Ni-based superconductors could be much higher than the values we observed for thin-film heterostructure samples. Oxygen vacancies are negligible in the  $\text{SrTiO}_3$  substrate of the superconducting  $\text{Nd}_{0.8}\text{Sr}_{0.2}\text{NiO}_2/\text{SrTiO}_3$  heterostructure. The surface topography obviously affects the normal-state transport properties of the  $\text{Nd}_{0.8}\text{Sr}_{0.2}\text{NiO}_2/\text{SrTiO}_3$  thin-film heterostructure but does not vary the superconducting parameters remarkably, which suggests that the superconducting properties of the nickelates could be, to some extent, independent of the normal state electron scattering for this new type of superconductivity. The out-of-plane negative magnetoresistance effect for the normal resistivity state is observed, which could be related to magnetic spins in the  $\text{Nd}_{0.8}\text{Sr}_{0.2}\text{NiO}_2$  thin film. In addition, the anisotropic critical fields for out-of-plane and in-plane magnetic fields could be a common feature for superconducting nanoscale thin-film heterostructures, simply due to the shape anisotropy and the resulting suppression of the orbital scattering. Our preliminary experiments indicate that the superconducting transition temperatures can be modulated by electrostatic doping. Finally, we hope that the experimental results could be helpful for understanding this intriguing electron system.

**Acknowledgements** Zhiqi Liu acknowledges financial support by the National Natural Science Foundation of China (Nos. 51822101, 51861135104 and 51771009).

## References

- [1] Li D, Lee K, Wang BY, Osada M, Crossley S, Lee HR, Cui Y, Hikita Y, Hwang HY. Superconductivity in an infinite-layer nickelate. *Nature*. 2019;572:624.
- [2] Hayward MA, Rosseinsky MJ. Synthesis of the infinite layer Ni(I) phase  $\text{NdNiO}_{2+x}$  by low temperature reduction of  $\text{NdNiO}_3$  with sodium hydride. *Solid State Sci*. 2013;5: 839.
- [3] Zhang FC, Rice TM. Effective Hamiltonian for the superconducting Cu oxides. *Phys Rev B*. 1988;37:3759.
- [4] Nomura Y, Hirayama M, Tadano T, Yoshimoto Y, Nakamura K, Arita R. Formation of a two-dimensional single-component correlated electron system and band engineering in the nickelate superconductor  $\text{NdNiO}_2$ . *Phys Rev B*. 2019;100:205138.
- [5] Jiang P, Si L, Liao Z, Zhong Z. Electronic structure of rare-earth infinite-layer  $\text{RNiO}_2$  ( $R = \text{La}, \text{Nd}$ ). *Phys Rev B*. 2019;100:201106(R).
- [6] Botana AS, Norman MR. Similarities and differences between  $\text{LaNiO}_2$  and  $\text{CaCuO}_2$  and implications for superconductivity. *Phys Rev X*. 2020;10:011024.
- [7] Zhang GM, Yang YF, Zhang FC. Self-doped Mott insulator for parent compounds of nickelate superconductors. *Phys Rev B*. 2020;101:020501(R).
- [8] Adhikary P, Bandyopadhyay S, Das T, Dasgupta I, Saha-Dasgupta T. Orbital-selective superconductivity in a two-band model of infinite-layer nickelates. *Phys Rev B*. 2020;102:100501(R).
- [9] Gu Y, Zhu S, Wang X, Hu J, Chen H. A substantial hybridization between correlated Ni-*d* orbital and itinerant electrons in infinite-layer nickelates. *Commun Phys*. 2020;3:84.
- [10] Geisler B, Pentcheva R. Fundamental difference in the electronic reconstruction of infinite-layer versus perovskite neodymium nickelate films on  $\text{SrTiO}_3(001)$ . *Phys Rev B*. 2020;102:020502(R).
- [11] Bandyopadhyay S, Adhikary P, Das T, Dasgupta I, Saha-Dasgupta T. Superconductivity in infinite-layer nickelates: Role of *f* orbitals. *Phys Rev B*. 2020;102: 220502(R).
- [12] He R, Jiang P, Lu Y, Song Y, Chen M, Jin M, Shui L, Zhong Z. Polarity-induced

electronic and atomic reconstruction at NdNiO<sub>2</sub>/SrTiO<sub>3</sub> interfaces. Phys Rev B. 2020;102:035118.

[13] Petocchi F, Christiansson V, Nilsson F, Aryasetiawan F, Werner P. Normal State of Nd<sub>1-x</sub>Sr<sub>x</sub>NiO<sub>2</sub> from Self-Consistent GW+EDMFT. Phys Rev X. 2020;10:041047.

[14] Nica EM, Krishna J, Yu R, Si Q, Botana AS, Erten O. Theoretical investigation of superconductivity in trilayer square-planar nickelates. Phys Rev B. 2020;102:020504(R).

[15] Leonov I, Skornyakov SL, Savrasov SY. Lifshitz transition and frustration of magnetic moments in infinite-layer NdNiO<sub>2</sub> upon hole doping. Phys Rev B. 2020;101:241108(R).

[16] Lechermann F. Late transition metal oxides with infinite-layer structure: Nickelates versus cuprates. Phys Rev B. 2020;101:081110(R).

[17] Lechermann F. Multiorbital processes rule the Nd<sub>1-x</sub>Sr<sub>x</sub>NiO<sub>2</sub> normal state. Phys Rev X. 2020;10:041002.

[18] Krishna J, LaBollita H, Fumega AO, Pardo V, Botana AS. Effects of Sr doping on the electronic and spin-state properties of infinite-layer nickelates: Nature of holes. Phys Rev B. 2020;102:224506.

[19] Katukuri VM, Bogdanov NA, Weser O, Brink J, Alavi A. Electronic correlations and magnetic interactions in infinite-layer NdNiO<sub>2</sub>. Phys Rev B. 2020;102:241112(R).

[20] Jiang M, Berciu M, Sawatzky GA. Critical Nature of the Ni Spin State in Doped NdNiO<sub>2</sub>. Phys Rev Lett. 2020;124:207004.

[21] Zhang Y, Lin LF, Hu W, Moreo A, Dong S, Dagotto E. Similarities and differences between nickelate and cuprate films grown on a SrTiO<sub>3</sub> substrate. Phys Rev B. 2020;102:195117.

[22] Werner P, Hoshino S. Nickelate superconductors: Multiorbital nature and spin freezing. Phys Rev B. 2020;101:041104(R).

[23] Wang Z, Zhang GM, Yang YF, Zhang FC. Distinct pairing symmetries of superconductivity in infinite-layer nickelates. Phys Rev B. 2020;102:220501(R).

[24] Wang Y, Kang CJ, Miao H, Kotliar G. Hund's metal physics: From SrNiO<sub>2</sub> to LaNiO<sub>2</sub>. Phys Rev B. 2020;102:161118(R).

- [25] Si L, Xiao W, Kaufmann J, Tomczak JM, Lu Y, Zhong Z, Held K. Topotactic Hydrogen in Nickelate Superconductors and Akin Infinite-Layer Oxides  $ABO_2$ . *Phys Rev Lett*. 2020;124:166402.
- [26] Ryee S, Yoon H, Kim TJ, Jeong MY, Han MJ. Induced magnetic two-dimensionality by hole doping in the superconducting infinite-layer nickelate  $Nd_{1-x}Sr_xNiO_2$ . *Phys Rev B*. 2020;101:064513.
- [27] Liu Z, Xu C, Cao C, Zhu W, Wang ZF, Yang J. Doping dependence of electronic structure of infinite-layer  $NdNiO_2$ . *Phys Rev B*. 2020;103:045103.
- [28] Wan X, Ivanov V, Resta G, Leonov I, Savrasov SY. Exchange interactions and sensitivity of the Ni two-hole spin state to Hund's coupling in doped  $NdNiO_2$ . *Phys Rev B*. 2020;103:075123.
- [29] Osada M, Wang BY, Goodge BH, Lee K, Yoon H, Sakuma K, Li D, Miura M, Kourkoutis LF, Hwang HY. A superconducting praseodymium nickelate with infinite layer structure. *Nano Lett*. 2020;20:5735.
- [30] Li D, Wang BY, Lee K, Harvey SP, Osada M, Goodge BH, Kourkoutis LF, Hwang HY. Superconducting Dome in  $Nd_{1-x}Sr_xNiO_2$  Infinite Layer Films. *Phys Rev Lett*. 2020;125:027001.
- [31] Lee K, Goodge BH, Li D, Osada M, Wang BY, Cui Y, Kourkoutis LF, Hwang HY. Aspects of the synthesis of thin film superconducting infinite-layer nickelates. *APL mater*. 2020;8:041107.
- [32] Wang BY, Li D, Goodge BH, Lee K, Osada M, Harvey SP, Kourkoutis LF, Beasley MR, Hwang HY. Isotropic Pauli-limited superconductivity in the infinite-layer nickelate  $Nd_{0.775}Sr_{0.225}NiO_2$ . *Nat Phys*. 2021; <https://doi.org/10.1038/s41567-020-01128-5>.
- [33] Gu Q, Li Y, Wan S, Li H, Guo W, Yang H, Li Q, Zhu X, Pan X, Nie Y, Wen HH. Single particle tunneling spectrum of superconducting  $Nd_{1-x}Sr_xNiO_2$  thin films. *Nat Commun*. 2020;11:6027.
- [34] Xiang Y, Li Q, Li Y, Yang H, Nie Y, Wen HH. Physical properties revealed by transport measurements on superconducting  $Nd_{0.8}Sr_{0.2}NiO_2$  thin films. *arXiv*:2007.04884.

- [35] Gao Q, Zhao Y, Zhou X, Zhu Z. Preparation of superconducting thin film of infinite-layer nickelate  $\text{Nd}_{0.8}\text{Sr}_{0.2}\text{NiO}_2$ . arXiv:2102.10292v2.
- [36] Zeng S, Tang CS, Yin X, Li C, Li M, Huang Z, Hu J, Liu W, Omar GJ, Jani H, Lim ZS, Han K, Wan D, Yang P, Pennycook SJ, Wee ATS, Ariando A. Phase diagram and superconducting dome of infinite-layer  $\text{Nd}_{1-x}\text{Sr}_x\text{NiO}_2$  thin films. *Phys Rev Lett.*2020;125,147003.
- [37] Zhou XR, Feng ZX, Qin PX, Yan H, Hu S, Guo HX, Wang XN, Wu HJ, Zhang X, Chen HY, Qiu XP, Liu ZQ. Absence of superconductivity in  $\text{Nd}_{0.8}\text{Sr}_{0.2}\text{NiO}_x$  thin films without chemical reduction. *Rare Met.*2020;39:368.
- [38] Liu ZQ, Leusink DP, Wang X, Lü WM, Gopinadhan K, Annadi A, Zhao YL, Huang XH, Zeng SW, Huang Z, Srivastava A, Dhar S, Venkatesan T, Ariando. Metal-insulator transition in  $\text{SrTiO}_{3-x}$  thin films induced by frozen-out carriers. *Phys Rev Lett.* 2011;107:146802.
- [39] Liu ZQ, Li CJ, Lü WM, Huang XH, Huang Z, Zeng SW, Qiu XP, Huang LS, Annadi A, Chen JS, Coey JMD, Venkatesan T, Ariando. Origin of the two-dimensional electron gas at  $\text{LaAlO}_3/\text{SrTiO}_3$  interfaces: The role of oxygen vacancies and electronic reconstruction. *Phys Rev X.* 2013;3:021010.
- [40] Huebener RP, Kampwirth RT, Martin RL, Barbee T, Zubeek RB. Critical Current Density in Superconducting Niobium Films. *J Low Temp Phys.*1975;19:247.
- [41] Chen Y, Bian W, Huang W, Tang X, Zhao G, Li L, Li N, Huo W, Jia J, You C. High critical current density of  $\text{YBa}_2\text{Cu}_3\text{O}_{7-x}$  superconducting films prepared through a DUV-assisted solution deposition process. *Sci Rep.*2016;6:38257.
- [42] Zhao Y, Feng Y, Cheng CH, Zhou L, Wu Y, Machi T, Fudamoto Y, Koshizuka N, Murakami M. High critical current density of  $\text{MgB}_2$  bulk superconductor doped with Ti and sintered at ambient pressure. *Appl Phys Lett.*2001;79:1154.
- [43] Pallecchi I, Tropeano M, Lamura G, Pani M, Palombo M, Palenzona A, Putti M. Upper critical fields and critical current densities of Fe-based superconductors as compared to those of other technical superconductors. *Physica C.*2012;482:68.
- [44] Li Q, He C, Si J, Zhu X, Zhang Y, Wen HH. Absence of superconductivity in bulk  $\text{Nd}_{1-x}\text{Sr}_x\text{NiO}_2$ . *Commun Mater.*2020;1:16.

- [45] Wang BX, Zheng H, Krivyakina E, Chmaissem O, Lopes PP, Lynn JW, Gallington LC, Ren Y, Rosenkranz S, Mitchell JF, Phelan D. Synthesis and characterization of bulk  $\text{Nd}_{1-x}\text{Sr}_x\text{NiO}_2$  and  $\text{Nd}_{1-x}\text{Sr}_x\text{NiO}_3$ . *Phys Rev Mater.*2020;4:084409.
- [46] He C, Ming X, Li Q, Zhu X, Si J, Wen HH. Synthesis and physical properties of perovskite  $\text{Sm}_{1-x}\text{Sr}_x\text{NiO}_3$  ( $x = 0, 0.2$ ) and infinite-layer  $\text{Sm}_{0.8}\text{Sr}_{0.2}\text{NiO}_2$  nickelates. *arXiv:2010.11777v2*.
- [47] Werthamer NR, Helfand E, Hohenberg PC. Temperature and purity dependence of the Superconducting Critical Field  $H_{c2}$ . III. Electron Spin and Spin-Orbit Effects. *Phys Rev.*1966;147:295.
- [48] Talantsev EF. In-plane  $p$ -wave coherence length in iron-based superconductors. *Results Phys.*2020;18:103339.
- [49] Yan H, Feng Z, Shang S, Wang X, Hu Z, Wang J, Zhu Z, Wang H, Chen Z, Hua H, Lu W, Wang J, Qin P, Guo H, Zhou X, Leng Z, Liu Z, Jiang C, Coey M, Liu Z. A piezoelectric, strain-controlled antiferromagnetic memory insensitive to magnetic fields. *Nat Nanotech.*2019;14:131.
- [50] Müller KA, Burkard H.  $\text{SrTiO}_3$ : An intrinsic quantum paraelectric below 4 K. *Phys Rev B.* 1979;19:3593.
- [51] Liu ZQ, Li L, Gai Z, Clarkson JD, Hsu SL, Wong AT, Fan LS, Lin MW, Rouleau CM, Ward TZ, Lee HN, Sefat AS, Christen HM, Ramesh R. Full electroresistance modulation in a mixed-phase metallic alloy. *Phys Rev Lett.* 2016;116:097203.
- [52] Liu ZQ, Chen H, Wang JM, Liu JH, Wang K, Feng ZX, Yan H, Wang XR, Jiang CB, Coey JMD, MacDonald AH. Electrical switching of the topological anomalous Hall effect in a non-collinear antiferromagnet above room temperature. *Nat Electron.* 2018;1:172.
- [53] Liu ZQ, Liu JH, Biegalski MD, Hu JM, Shang SL, Ji Y, Wang JM, Hsu SL, Wong AT, Cordill MJ, Gludovatz B, Marker C, Yan H, Feng ZX, You L, Lin MW, Ward TZ, Liu ZK, Jiang CB, Chen LQ, Ritchie RO, Christen HM, Ramesh R. Electrically reversible cracks in an intermetallic film controlled by an electric field. *Nat Commun.* 2018;9:41.
- [54] Yan H, Feng Z, Qin P, Zhou X, Guo H, Wang X, Chen H, Zhang X, Wu H, Jiang

C, Liu Z. Electric-field-controlled antiferromagnetic spintronic devices. *Adv Mater.* 2020;32:1905603.

[55] Guo H, Feng Z, Yan H, Liu J, Zhang J, Zhou X, Qin P, Cai J, Zeng Z, Zhang X, Wang X, Chen H, Wu H, Jiang C, Liu Z. Giant piezospintronic effect in a noncollinear antiferromagnetic metal. *Adv Mater.* 2020;32:2002300.

[56] Qin P, Feng Z, Zhou X, Guo H, Wang J, Yan H, Wang X, Chen H, Zhang X, Wu H, Zhu Z, Liu Z. Anomalous Hall Effect, Robust negative magnetoresistance, and memory devices based on a noncollinear antiferromagnetic metal. *ACS Nano.* 2020;14:6242.

[57] Wang X, Feng Z, Qin P, Yan H, Zhou X, Guo H, Leng Z, Chen W, Jia Q, Hu Z, Wu H, Zhang X, Jiang C, Liu Z. Integration of the noncollinear antiferromagnetic metal Mn<sub>3</sub>Sn onto ferroelectric oxides for electric-field control. *Acta Mater.* 2019;181:537.

[58] Feng Z, Qin P, Yang Y, Yan H, Guo H, Wang X, Zhou X, Han Y, Yi J, Qi D, Yu X, Breese MBH, Zhang X, Wu H, Chen H, Xiang H, Jiang C, Liu Z. A two-dimensional electron gas based on a 5s oxide with high room-temperature mobility and strain sensitivity. *Acta Mater.* 2021;204:116516.

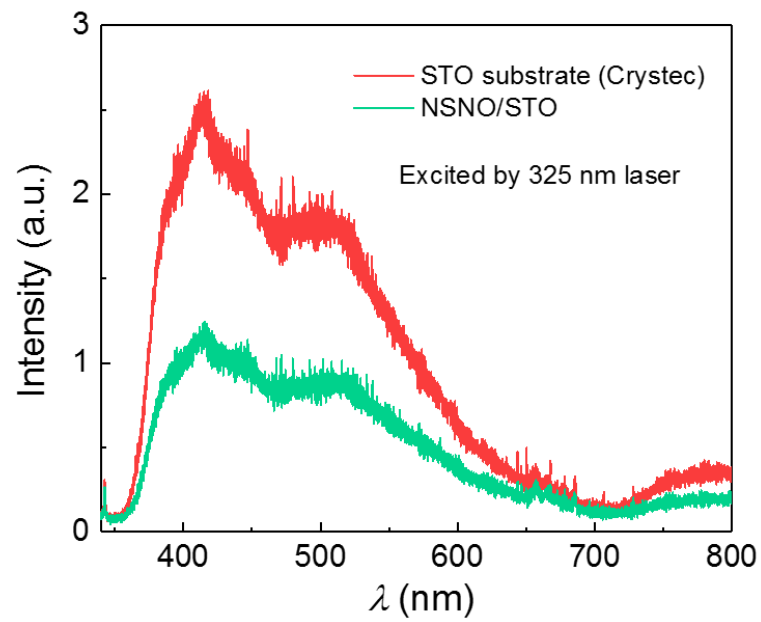
[59] Qin PX, Yan H, Wang XN, Feng ZX, Guo HX, Zhou XR, Wu HJ, Zhang X, Leng ZGG, Chen HY, Liu ZQ. Noncollinear spintronics and electric-field control: a review. *Rare Met.* 2020;39:95.

[60] Feng Z, Yan H, Liu Z. Electric-field control of magnetic order: From FeRh to topological antiferromagnetic spintronics. *Adv Electron Mater.* 2019;5:1800466.

[61] Liu Z, Feng Z, Yan H, Wang X, Zhou X, Qin P, Guo H, Yu R, Jiang C. Antiferromagnetic piezospintronics. *Adv Electron Mater.* 2019;5:1900176.

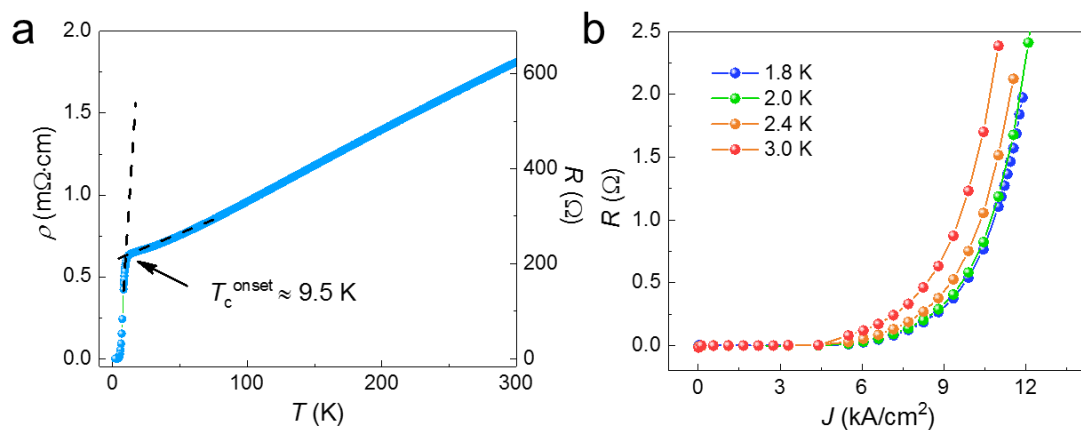
[62] Xi XX, Li Q, Doughty C, Kwon C, Bhattacharya S, Findikoglu AT, Venkatesan T. Electric field effect in high  $T_c$  superconducting ultrathin YBa<sub>2</sub>Cu<sub>3</sub>O<sub>7-x</sub> films. *Appl Phys Lett.* 1991;59:3470.

**Figure 1**



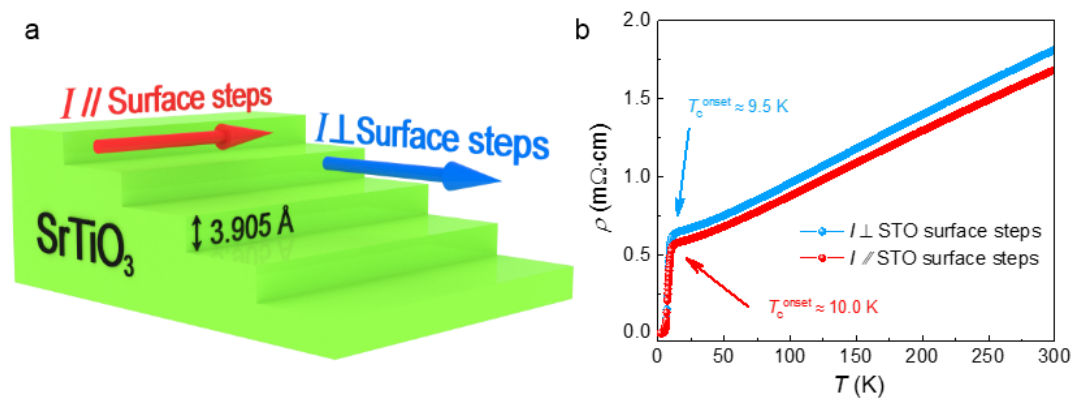
**Fig. 1** Room-temperature photoluminescence of a bare SrTiO<sub>3</sub> (STO) substrate purchased from Crystec and a superconducting Nd<sub>0.8</sub>Sr<sub>0.2</sub>NiO<sub>2</sub>/SrTiO<sub>3</sub> (NSNO/STO) heterostructure excited by 325 nm laser.

**Figure 2**



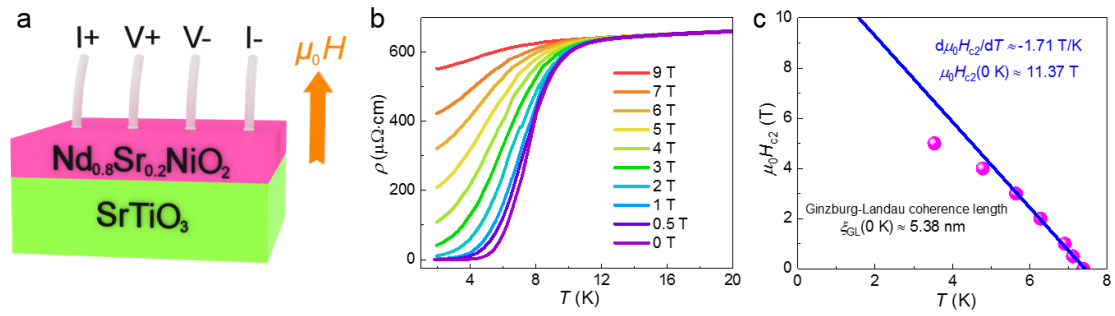
**Fig. 2 a** Temperature-dependent resistivity of a 14-nm-thick  $Nd_{0.8}Sr_{0.2}NiO_2/SrTiO_3$  thin-film heterostructure; **b** current density dependent resistance of the  $Nd_{0.8}Sr_{0.2}NiO_2/SrTiO_3$  heterostructure at different temperatures.

**Figure 3**



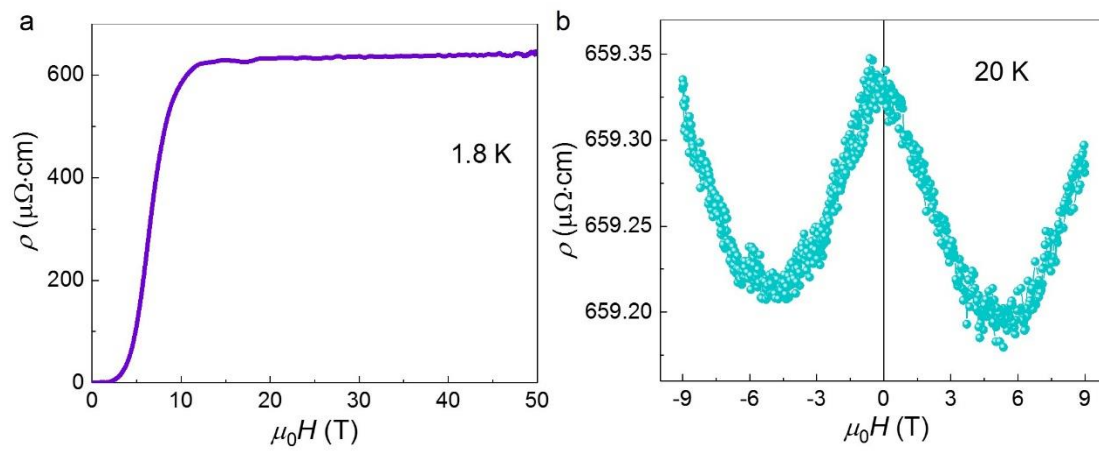
**Fig. 3 a** Schematic of the measurement geometry for different current directions; **b** temperature-dependent resistivity of the Nd<sub>0.8</sub>Sr<sub>0.2</sub>NiO<sub>2</sub>/SrTiO<sub>3</sub> heterostructure measured by different current directions.

**Figure 4**



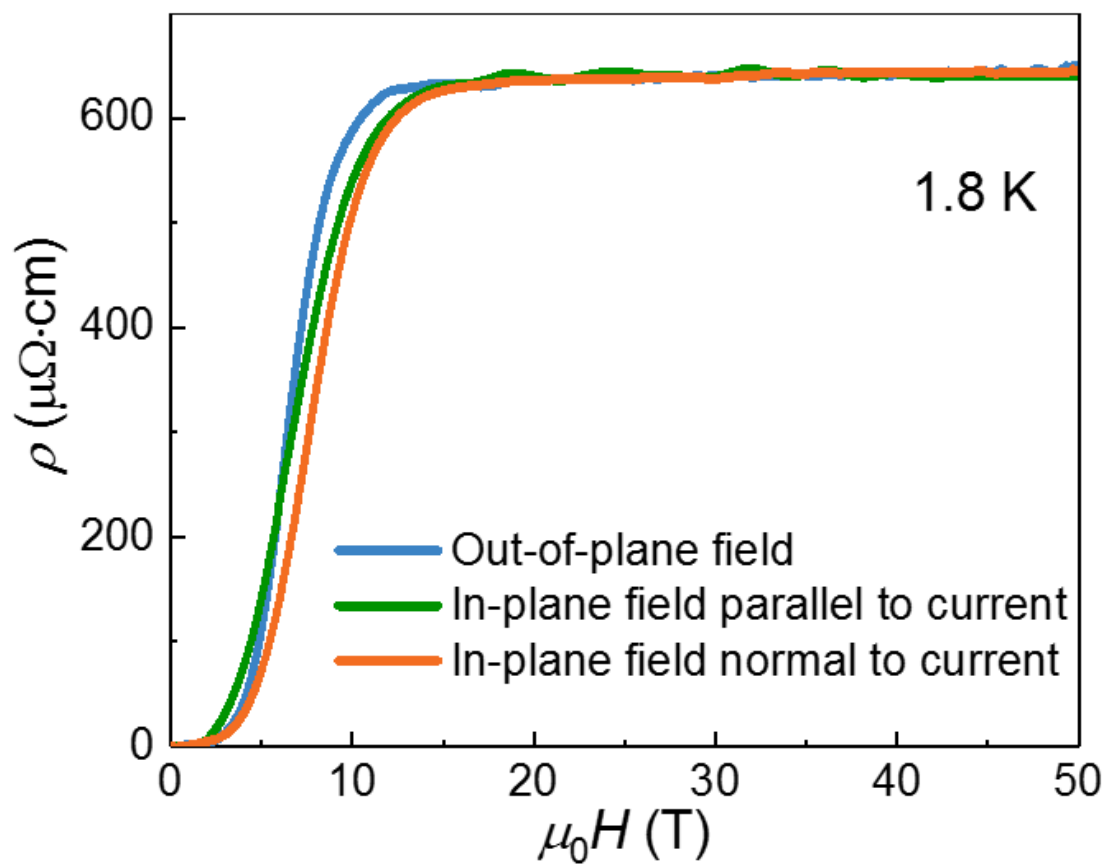
**Fig. 4 a** Schematic of the measurement geometry for the out-of-plane magnetotransport; **b** temperature-dependent resistivity of the  $\text{Nd}_{0.8}\text{Sr}_{0.2}\text{NiO}_2/\text{SrTiO}_3$  heterostructure under different magnetic fields ranging from 0 to 9 T; **c** the upper critical field as a function of the temperature

**Figure 5**



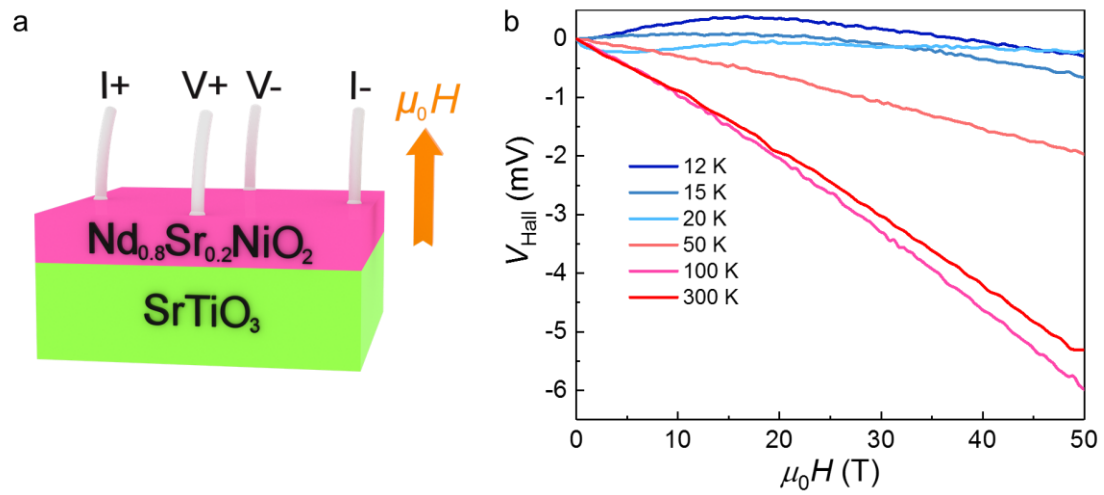
**Fig.5 a** Resistivity as a function of magnetic field up to 50 T at 1.8 K; **b** static-field magnetoresistance up to 9 T for the normal state at 20 K.

Figure 6



**Fig. 6** Resistivity as a function of magnetic field up to 50 T at 1.8 K for three measurement geometries between the measuring current and the magnetic field.

**Figure 7**



**Fig. 7 a** Cartoon illustration for the Hall measurement connections; **b** Hall voltage versus magnetic field up to 50 T for the normal state above 10 K.

**Figure 8**

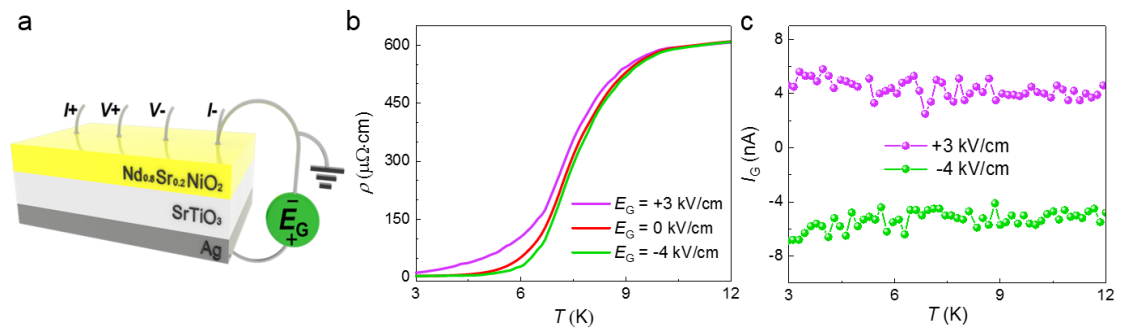


**Fig. 8** **a** Schematic of the measurement geometry of the electric-field modulation experiment; **b** Superconducting transition for different gating electric fields  $E_G$ ; **c** Perpendicular gating current versus temperature under different gating electric fields.